NASA Technical Memorandum 101727

Techniques for Hot Structures Testing

V. Michael DeAngelis and Roger A. Fields

November 1990

National Aeronautics and
Space Administration

NASA Technical Memorandum 101727

Techniques for Hot Structures Testing

V. Michael DeAngelis and Roger A. Fields
NASA Ames Research Center, Dryden Flight Research Facility, Edwards, California

1990

National Aeronautics and
Space Administration
Ames Research Center
Dryden Flight Research Facility
Edwards, California 93523-0273

TECHNIQUES FOR HOT STRUCTURES TESTING

V. Michael DeAngelis
Aerostructures Branch
NASA Ames Research Center
Dryden Flight Research Facility
Edwards, CA 93523-0273

Roger A. Fields
Aerostructures Branch
NASA Ames Research Center
Dryden Flight Research Facility
Edwards, CA 93523-0273

Hot structures test techniques developed and applied by the Aerostuctures Branch of the NASA Ames Research Center, Dryden Flight Research Facility are presented. Topics covered include the data acquisition and control of testing, the quartz lamp heater systems, current strain and temperature sensors, and hot structures test techniques used to simulate the flight thermal environment in the laboratory.

INTRODUCTION

At NASA Ames Research Center, Dryden Flight Research Facility, the Aerostructures Branch personnel have been involved with hot structures testing since the early 1960's beginning with the Mach 6, X-15 airplane. Early hot structures test programs at NASA Ames-Dryden focused on the operational testing required to support the X-15 flight test program, such as developing and demonstrating structural fixes to prevent the nose and main landing gear from deploying in flight at Mach 4, qualifying the canopy hooks under thermal load, and qualifying the ball nose airdata sensor system. Early hot structures research projects focused on developing laboratory test techniques to accurately simulate the flight thermal profiles [1–2]. Duplication of the flight aerodynamic heating in the laboratory was essential to identifying the thermal response of the calibrated strain gage instrumentation that was installed in the aircraft for the purpose of measuring airloads or structural loads. Once the thermal response of the calibrated strain gages was determined from the laboratory tests, then the resulting flight airloads or structural loads could be determined [3–5].

At the conclusion of the X-15 flight test program, laboratory tests on a horizontal stabilizer and wing panel were instrumental in developing the thermal loads simulation techniques that were eventually applied to the YF-12A airplane. The YF-12A airplane was the latest hot structures flight vehicle involved in a major thermal loads research program, and the culmination of this research program is extensively documented [6]. Subsequent to the X-15 and YF-12A flight programs, the Aerostructures Branch personnel have been involved in numerous hot structures test programs to develop test methods and measurement techniques that focused on providing test data for correlation with results from analytical codes. In November 1988, the Aerostructures Branch at NASA Ames-Dryden, with participation from Langley Research Center, sponsored a three-day workshop that focused on the correlation of hot structures test data with analysis. The purpose was to provide a means to quickly disseminate the results of over two decades of experience with hot structures testing to members of the technical community. A summary of the workshop was published [7].

This paper will draw limited material from the workshop and provide a more formal documentation of topics that focus on hot structures test techniques employed at the Aerostructures Branch at NASA Ames-Dryden. Topics covered include the test data acquisition and control system, the quartz lamp heater systems, current strain and temperature sensors, and hot structures test techniques used to simulate the flight thermal environment in the laboratory.

Recognition is given to the Structures Test Branch at the Wright Research and Development Center, which has also contributed immensely to the development of hot structures test methods. The work has included both graphite heater systems and Vortek heater systems (Vortek Industries, Ltd., Vancouver, BC, Canada) that provide higher heat fluxes and temperatures than quartz lamp heater systems. No attempt to cover testing with these systems is made in this paper.

DATA SYSTEMS

Data acquired often differ in some degree from expected results. One reason for this occurrence is the use of practical data acquisition and control equipment that cause data deterioration. This arises because of uncertainties that creep into measurements provided by the equipment. The data acquisition and control system in service at NASA Ames-Dryden was designed to minimize these uncertainties. This section describes the system features.

Figure 1 shows an overview block diagram of the data acquisition and control system (DACS) used in NASA Ames-Dryden's Thermostructures Research Facility. Transducers are appropriately attached to a

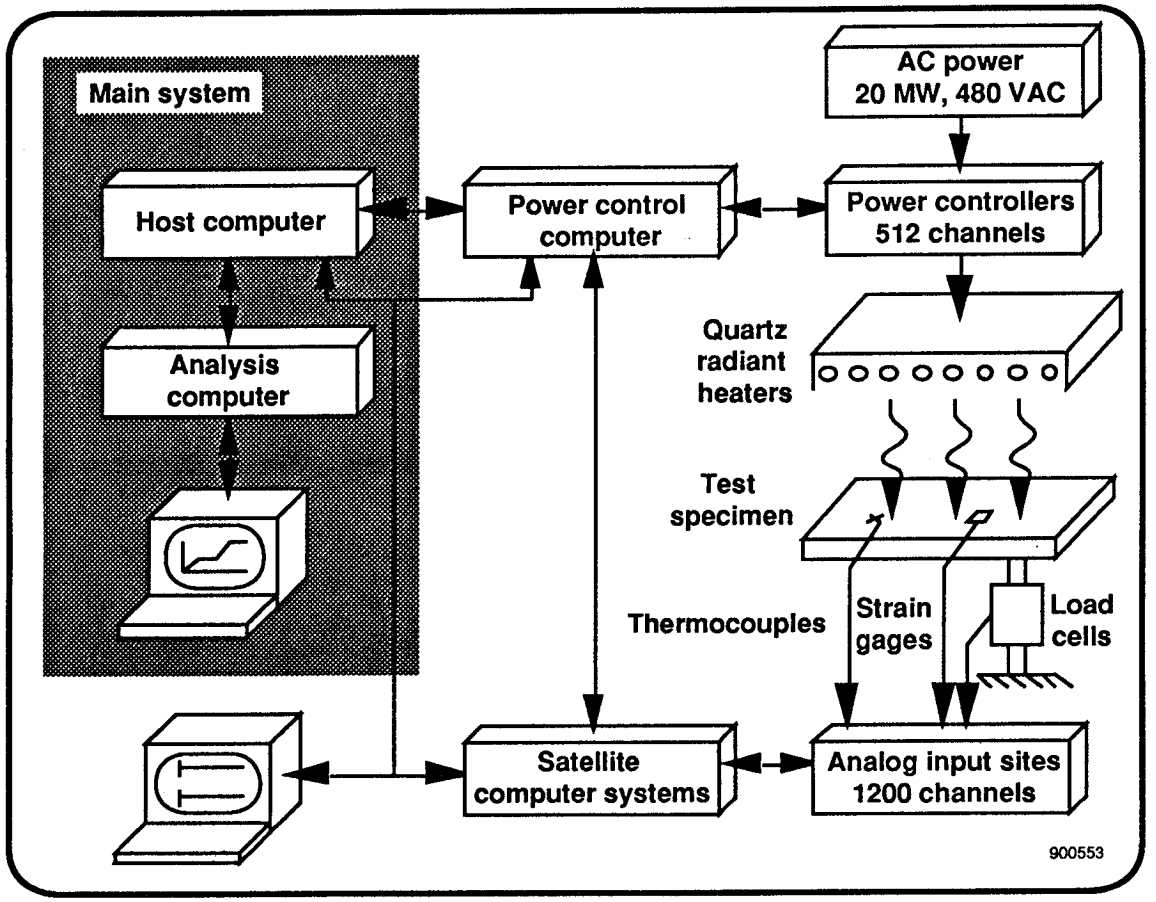

Fig. 1 DACS block diagram.

test specimen whereby analog input sites receive the transducer lead wires and take the measurements of the response to the test environment imposed. The information obtained is sent to a satellite computer system which provides information for real-time analysis monitoring and operational monitoring and control. Information is also sent to the power control computer which distributes the requests for power-level changes that cause a particular temperature control zone to approach the desired temperature as a function of time. There are 512 power control channels available, 20 MW of electrical power available to apply to a test set-up, and 1280 channels of data acquisition available. The main computer system is the "brain" behind the DACS. It is used to acquire and process data from three satellite systems, provide real-time displays of processed data, and to control the activities of the thermal and mechanical loads control systems. The DACS has been designed to provide closed-loop control on temperature measured by type K, type S, type J, and type B thermocouples.

The temperature control system of the DACS, like all closed-loop temperature control systems, can only operate in accordance with the feedback it receives. Therefore, the controlled temperature will be at the point of the feedback measurement on the test article, with neighboring areas differing in temperature from the feedback point. There are control errors and errors caused by feedback uncertainty. The control error refers to the inability of the control system to do a perfect job of matching the commanded temperature to the indicated temperature for the control channel. The indicated temperature has its own set of uncertainties related to thermocouple wire manufacturing tolerances, data acquisition tolerances, and data processing tolerances. Figure 2 depicts the control performance specification for the DACS system used in the Thermostructures

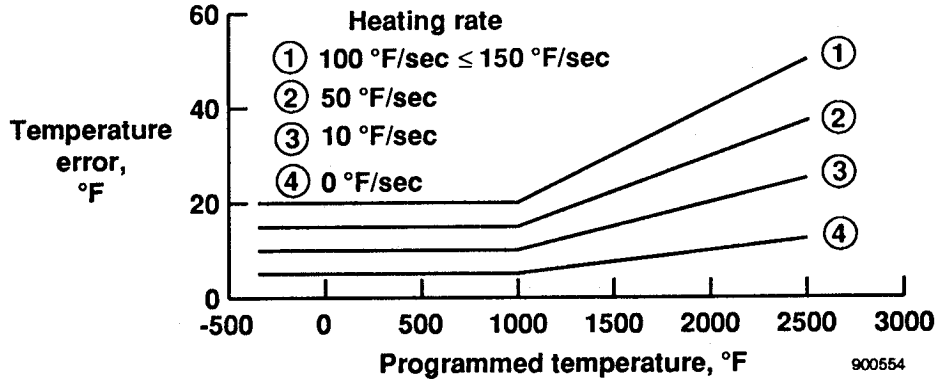

Fig. 2 DACS temperature control performance.

Research Facility. The heating rates range from 0 °F/sec, or a steady hold temperature, to 150 °F/sec, which is the maximum heating rate of the system. Notice that at lower temperatures and at lower temperature rates of change, the system performance errors are smaller. The closed-loop thermal control process is updated four times a second. Data recording rates can be varied from 1 sample/sec to 12 samples/sec for all 1280 channels. However, to acquire highly transient data, rates as high as 150 samples/sec have been achieved using a limited number of channels.

Figure 3 shows the DACS control performance for a nominal flight profile of a hypersonic vehicle that achieves a maximum temperature of 900 °F with a maximum heating rate of 20 °F/sec. The DACS does an excellent job of control with deviations typically under ±4 °F for the temperature profile shown.

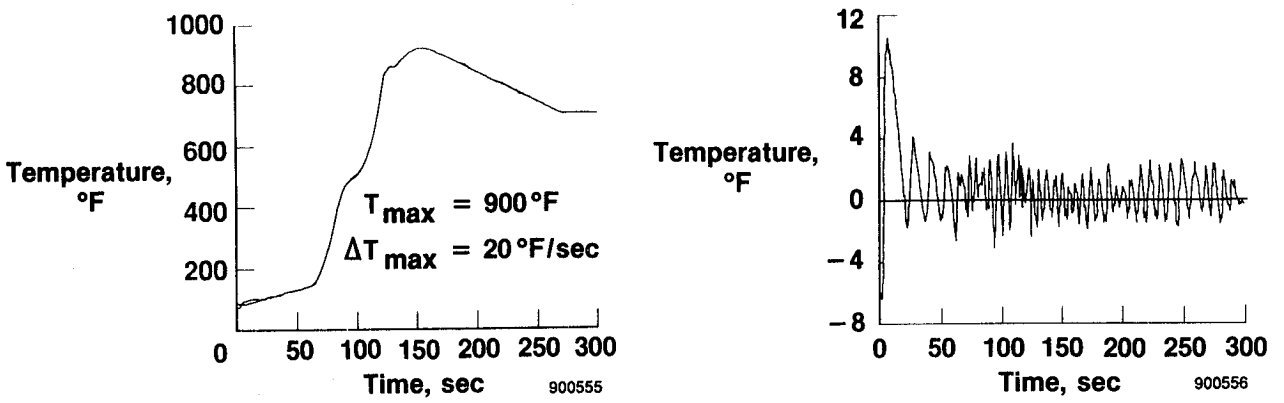

(a) Profile and measured data.

(b) Deviation from profile.

Fig. 3 Thermal test data.

For effective real-time monitoring of large tests, that is, tests with many control zones, such as the 470 separate temperature profiles required to heat the YF-12A airplane, the deviations of Fig. 3(b) are displayed in a bar-chart format as shown in Fig. 4. This display enables the test engineer to effectively monitor all of

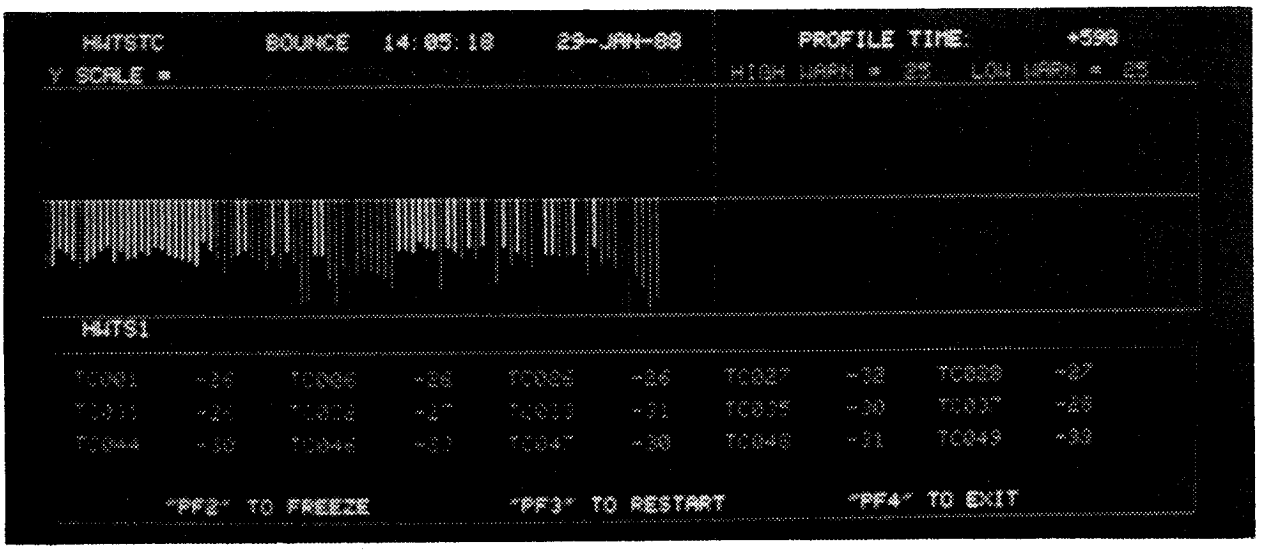

Fig. 4 Bar-chart display of profile deviations.

the heating zones, simultaneously. Should the deviations from the prescribed profiles exceed predetermined limits, the bars first change color. Then if the temperature is not brought under satisfactory control and the deviations become even larger, the system will automatically shut down. The data shown in Fig. 4 are taken from a heating test of the hypersonic wing test structure (HWTS) after the power to the quartz lamps was intentionally turned off. The data from the 89 control thermocouples show, as expected, that all of the zones are at temperatures below the desired, or programmed, temperature profile. A more detailed description of the DACS has been published [8].

INSTRUMENTATION

Thermocouples and strain gages are the principle sensors used in hot structures testing to measure temperature and strain, respectively. Figure 5 summarizes the temperature range and associated error limits for

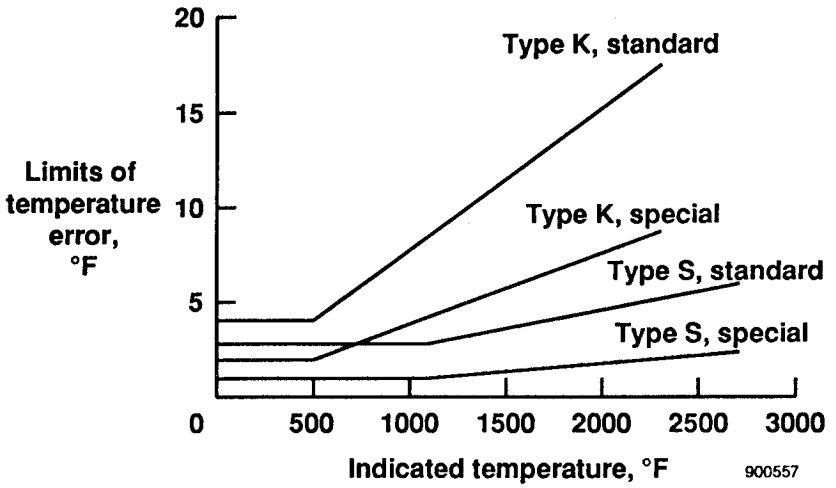

Fig. 5 Thermocouple specifications.

the type K and type S thermocouples. Development of an infrared sensor system for temperature measurement and thermal control is underway for use on test articles on which attachment of thermocouples has not been fully successful, such as carbon-carbon structures. Results of this work are beyond the scope of this paper.

Table 1 shows information on the strain gages used at NASA Ames-Dryden, including the method used for attachment, the temperature range to which they were subjected during testing, and the signal conditioning used. The current approximate cost of each gage is also shown, since that factor tends to influence the selection of the gage. Extensive experience has been gained in the use of foil, weldable, and capacitive gages over a wide range of temperatures. Two types of iron-chromium-aluminum (Fe-Cr-Al) alloy high-temperature gages (BCL-3 and ME II NZ 2100) are presently undergoing their first application on a laboratory structure.

Table 1. Strain gages used in hot structures testing.

Type	Method of attachment	Temperature range, °F	Signal conditioning	Approximate cost, each gage
Foil	Adhesive	−320 to 600	DC	$20
Weldable	Spot welding	−320 to 1,200	DC	$700
Capacitive	Spot welding	−320 to 1,500	AC ($1,000)	$1,500
Fe-Cr-Al alloy	Plasma–flame spray	70 to 1,900	DC	20 to 200

When applied to a hot structure, strain gage accuracy is dependent upon several factors including the gage factor and its change with temperature, the drift of the gage, and the apparent strain characteristics of the gage when applied to the test article material. Satisfactory gage factor and drift characteristics have been demonstrated for the foil, weldable, and capacitive gages. Limited data on the Fe-Cr-Al alloy gages also suggest satisfactory gage factor and drift characteristics [9]. The apparent strain then becomes the gage characteristic

that has the greatest impact on the accuracy of strain measurement at elevated temperature. Often the apparent strain can be much larger than the intended strain measurement. The apparent strain for resistance gages is a function of the difference between the coefficient of thermal expansion of the gage and the material to which it is attached, and the change in resistivity of the gage with change in temperature. Because of its design the capacitive gage (Fig. 6) has no significant apparent strain. Since the rod material and the test material

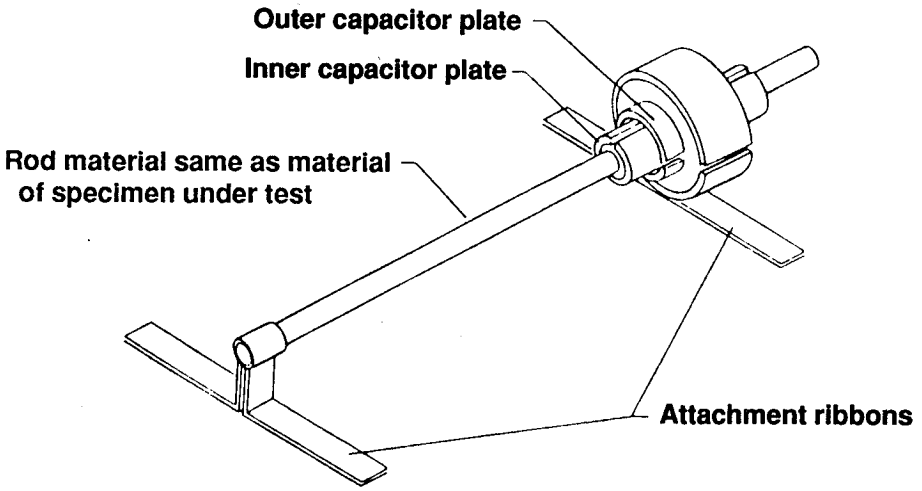

Fig. 6 High-temperature capacitive strain gage.

are the same, no apparent strain corrections should be needed. But because the rod is positioned off the surface of the test article, there is usually a difference in temperature between the rod and the surface which can produce a measurement error. A thermocouple attached to the rod and a thermocouple attached to the test article directly below the rod provide temperatures to compute the temperature difference used to correct the strain data.

Apparent strain tests must be performed prior to testing any structure that is instrumented with strain gages to measure strain or stress at elevated temperature. For foil gages, these tests consist of mounting several strain gages from a common batch on a sample material of the test article. The sample material or coupon is then heated slowly to achieve a thermal-stress-free temperature rise after which the coupon is allowed to cool slowly. Several cycles are run and the data are collected and analyzed. Typical apparent

strain curves for resistance gages are shown in Fig. 7. Figure 7(a) shows the apparent strain curves, from room temperature to 500 °F, for eight foil gages attached to a titanium coupon. As seen in the figure, the

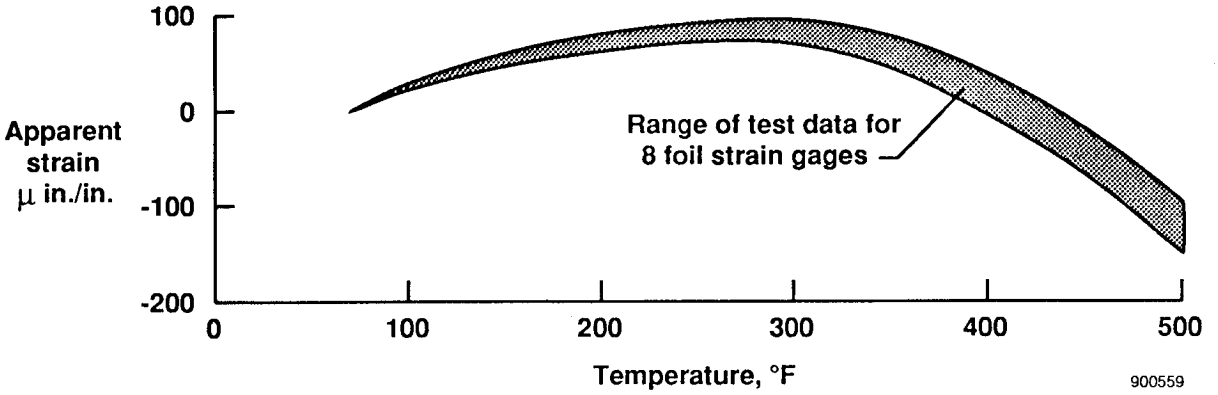

(a) Foil gages.

Fig. 7 Apparent strain curves for resistance gages.

foil strain gages exhibited little variation in apparent strain among the eight sensors. The apparent strain variation with temperature seen in these tests corresponded closely to the manufacturer's prediction.

Weldable strain gages also tend to generate repeatable apparent strain curves for multiple thermal cycles. However, the curves tend to vary widely from gage to gage as shown in Fig. 7(b) by the range of apparent

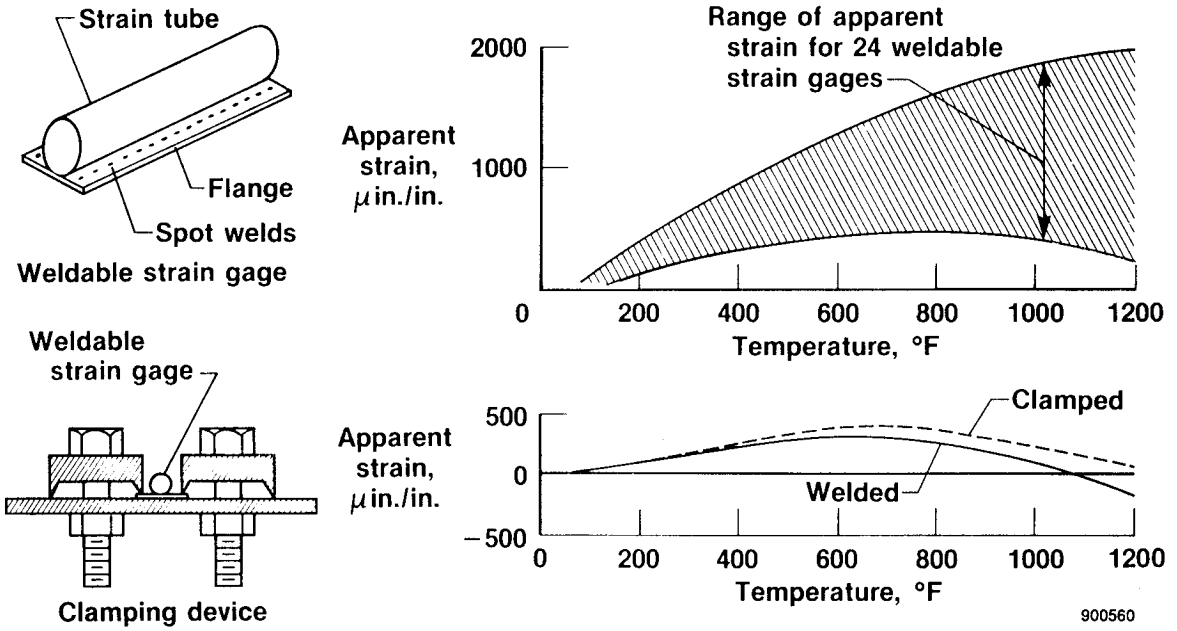

(b) Weldable gages.

Fig. 7 Continued.

strain for 24 weldable strain gages. The figure also depicts a method to establish an apparent strain curve for each gage before it is welded to the test article. A clamping device is manufactured from the same material

as that to which the gage will be attached. Then, using the clamping device as a test coupon, apparent strain curves are obtained for each gage to be used. This approach may seem to be tedious and costly, but it is necessary to obtain accurate strain measurements when using these gages at high temperatures.

The magnitude of the apparent strain varies for different Fe-Cr-Al alloy gages depending on the material to which they are attached. However, the characteristic behavior of the apparent strain with temperature is the same, since these types of gages are manufactured from the same basic material. Figure 7(c) represents

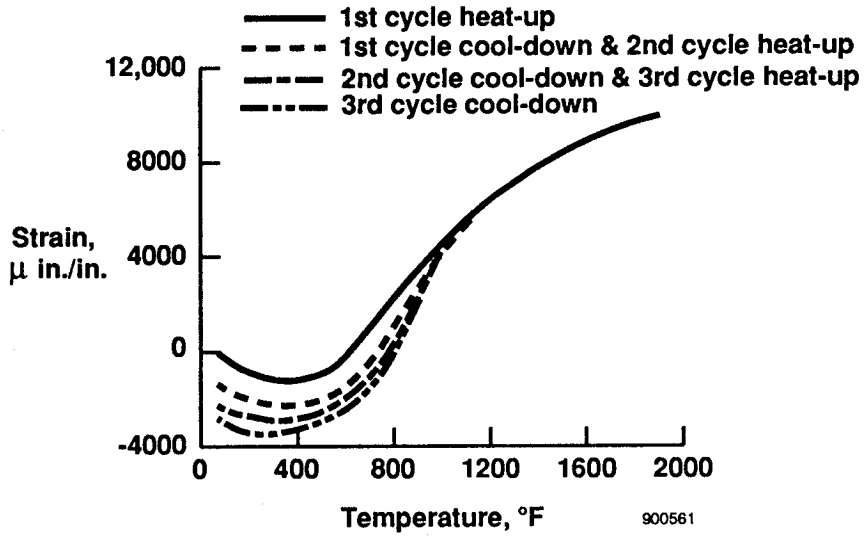

(c) Fe-Cr-Al alloy gages.

Fig. 7 Concluded.

data obtained from laboratory tests of one of these gages and these data are used to demonstrate their unique behavior. This figure shows the apparent strain for three heat-up and cool-down cycles over a temperature range from room temperature to 1900 °F. The gages were mounted on an Inconel 601 bar (Inco Alloys International, Inc., Huntington, WV). As seen in the figure, the second cycle heat-up traces the first cycle cool-down and the third cycle heat-up traces the second cycle cool-down. This characteristic exists because the strain at the maximum temperature is invariant, and essentially all metallurgical phase transformations occur during the cool-down portion of the cycle below about 1200 °F. Furthermore, as more cycles are run, the data for both heat-up and cool-down cycles converge into one curve. Test data show [9] a maximum deviation of 160 μ in./in. between the first cycle cool-down and the second cycle heat-up. The large apparent strain values suggest that generating apparent strain data from coupon tests to correct data from gages installed on a test panel is not a valid procedure. In addition, individual apparent strain curves must be generated from each gage as installed on the test structure. If this is indeed a requirement, then the scope of test programs in which these gages can be used is very limited. However, these gages are currently being used in a force-stiffness technique for measuring the buckling load on a buckling-critical panel. In this application, mechanical loads are applied after the panel is stabilized at an elevated temperature. Therefore, apparent strain is not a factor. Reference [9] contains a more thorough presentation and comparison of the unique characteristics of the Fe-Cr-Al alloy gages.

QUARTZ LAMP HEATING SYSTEM

Presently, quartz lamps are used exclusively to heat the test articles in the Thermostructures Research Facility. This section presents a simple, but relatively accurate method to calculate the available heat flux

for infrared radiation heating systems. Also discussed is the importance of test specimen emissivity on the power required.

Figure 8 presents the characteristics of the 200 W/in. T-3 quartz lamp. The values shown are for a lamp with a 10-in.-lighted length. By multiplying the values shown by the ratio of lamp length, this figure can be

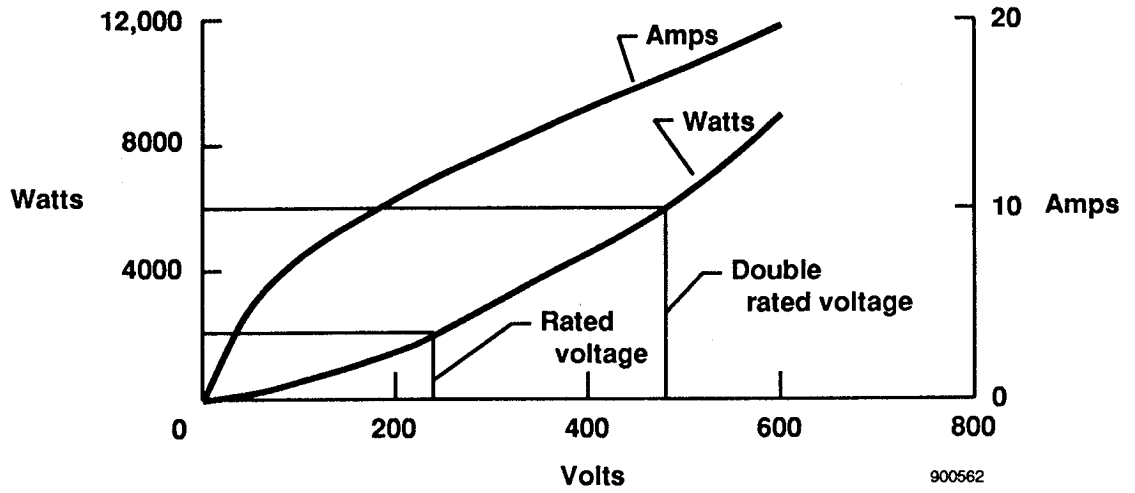

Fig. 8 Characteristics of 200 W/in., T-3, 10-in. quartz lamps.

used for 200 W/in. T-3 lamps of other lengths. As shown, this lamp produces 2000 W at rated voltage and 6000 W at double rated voltage.

The equation for calculating the available heat flux for an infrared radiation heater is

$$q_A = q_{max}(q_{T_0}/q_{T_n}) - q_{loss} - q_{end\,eff} \qquad (1)$$

where

q_{max} = maximum power output of the quartz lamps in Btu/ft^2-sec

q_{T_0}/q_{T_n} = ratio of radiant heat flux from the lamp filament at a specimen temperature of T_0 to the heat flux received by a specimen at a temperature of T_n

q_{loss} = heat flux loss of heater system in Btu/ft^2-sec

$q_{end\,eff}$ = end-effects heat flux loss due to heater design in Btu/ft^2-sec

The ratio of radiant heat flux (q_{T_0}/q_{T_n}) is derived from the difference between the surface temperature of the test specimen and the filament temperature of the quartz lamp. This ratio is shown in Fig. 9.

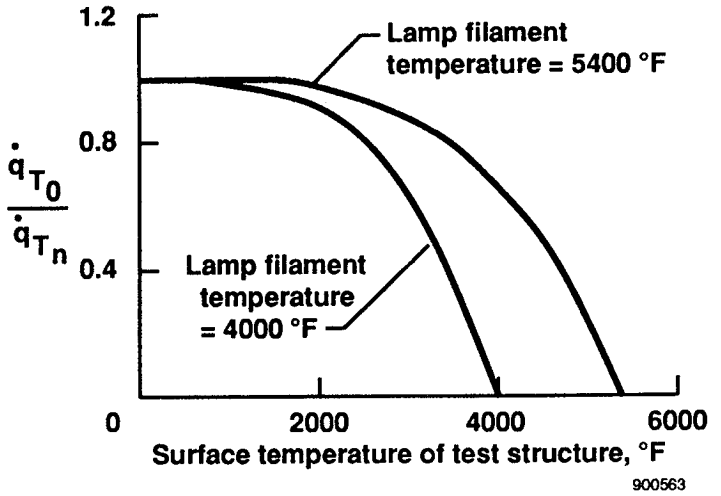

Fig. 9 Ratio of radiant heat flux.

A filament temperature of 4000 °F exists for quartz lamps that are operated at rated voltage (240 V), and 5400 °F is the filament temperature when the lamps are operated at double rated voltage (480 V). The ratio of radiant heat flux (q_{T_0}/q_{T_n}) times the maximum power output of the quartz lamps (q_{max}) represents the maximum possible available heat flux for a perfect heating system with zero losses.

The heat flux loss of the heater system (q_{loss}) includes the losses caused by radiation, conduction, and convection. Usually, each of these losses has to be calculated separately. These calculations are not free from errors since it is necessary to make several assumptions to perform the calculations. To circumvent the time-consuming process of calculation of heat losses resulting from each mode of heat transfer, an empirical curve of the total heat flux loss as a function of specimen temperature was derived from past heating tests using water-cooled polished aluminum reflectors and stainless steel reflectors. This curve is shown in Fig. 10 and is based on a specimen emissivity of approximately 0.85. Since the heating tests used to derive this

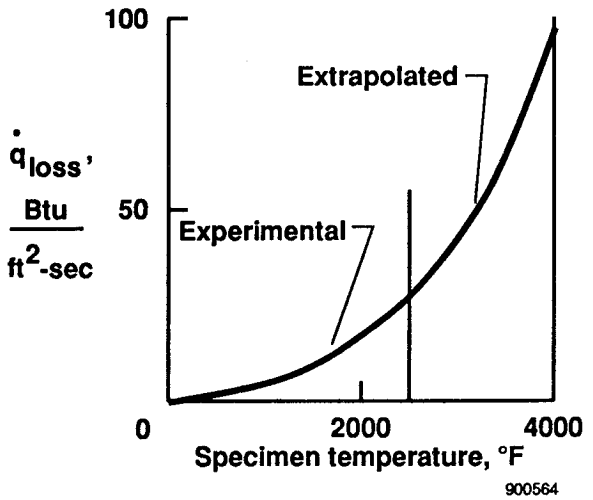

Fig. 10 Heat flux loss.

curve were conducted to only 2500 °F, the curve is verified up to that temperature only, and the part of the curve from 2500 °F to 4000 °F is an extrapolation. As previously mentioned, this curve represents the total heating loss from radiation, conduction, and convection, but does not consider heat loss caused by end effects. Heat loss resulting from end effects (boundary conditions) will be discussed in a subsequent section.

Figure 11 shows the power required as a function of heater area for specimen temperatures up to 3800 °F and heating rates from steady state (SS) up to 10 Btu/ft^2-sec. The calculations were made for a specimen emissivity of 0.85. At very high temperatures (3500 °F to 3800 °F), the slope of the curve is such that the heater area is quite small. In the Thermostructures Research Facility the maximum power available is 20 MW.

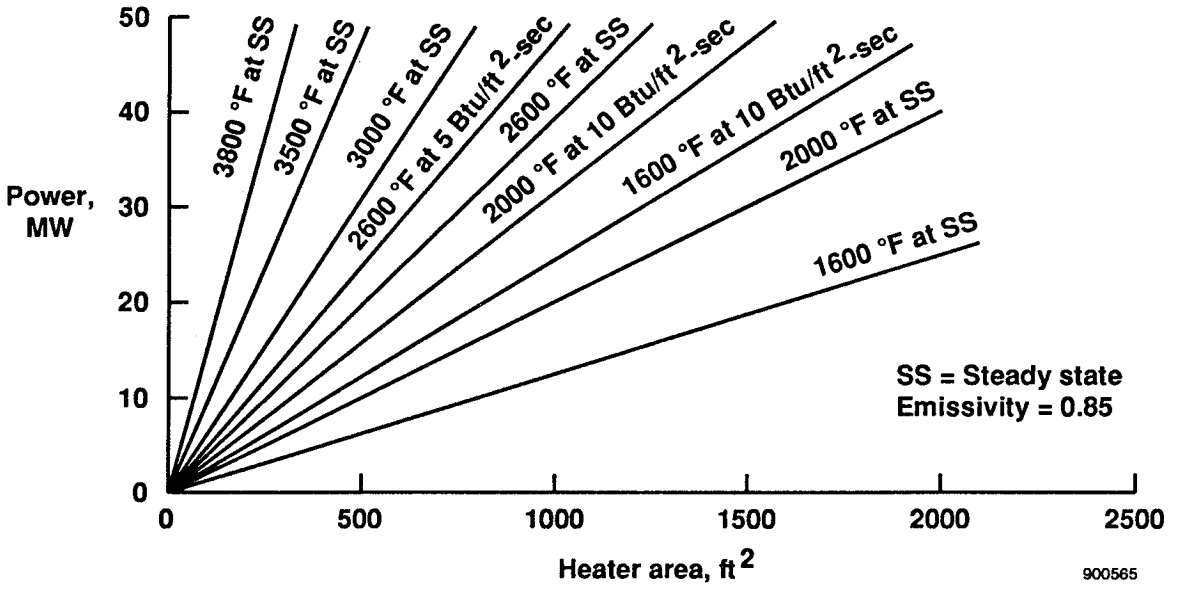

Fig. 11 Power required as a function of heater area.

HOT STRUCTURES TEST TECHNIQUES

Several important topics, which are directly related to testing with infrared quartz heaters, will be addressed in this section. A combination of laboratory test, flight test, and analytical data from a variety of sources is presented in addressing control zone sizing for quartz lamp heating, quartz lamp distribution, test specimen surface emissivity effects, and boundary conditions for thermal testing.

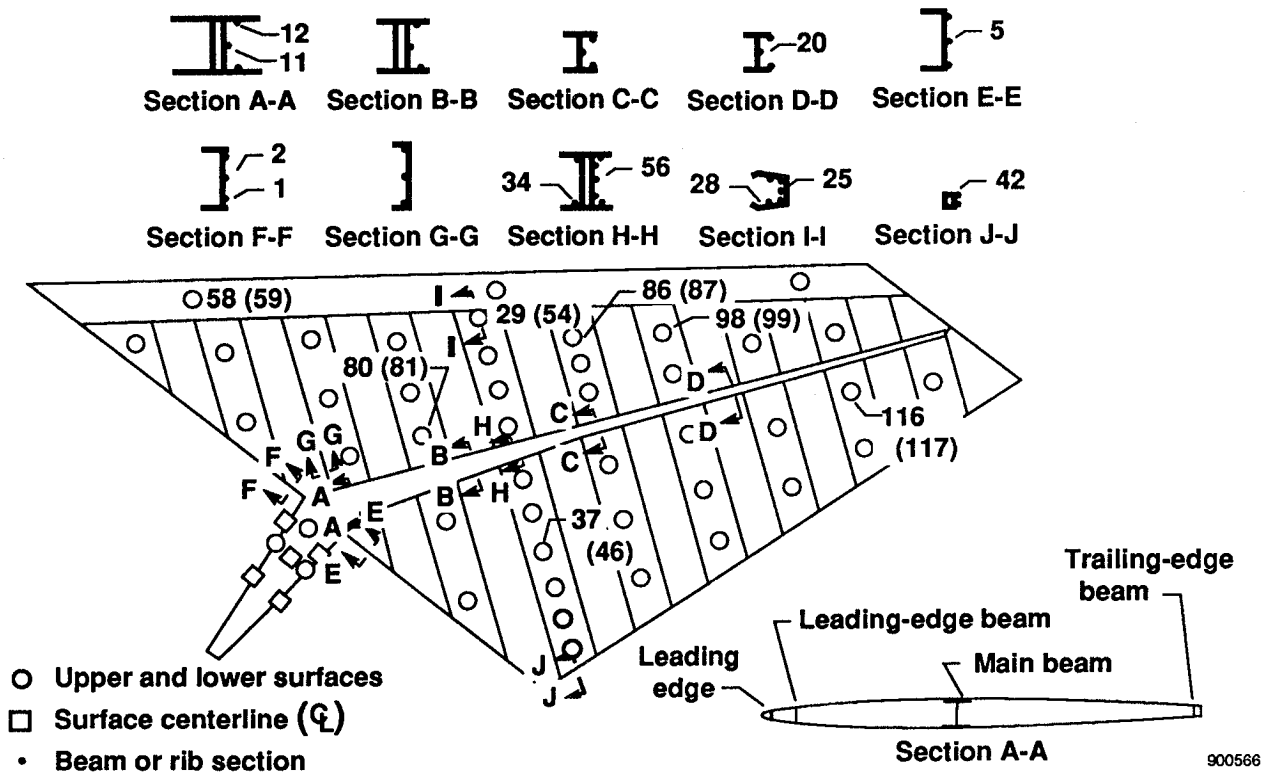

Fig. 12 X-15 horizontal stabilizer structure with thermocouple locations.

The X-15 horizontal stabilizer, shown in Fig. 12, was of conventional semimonocoque construction. Although Inconel-X was the primary material, the aft ribs and trailing-edge beam were a titanium alloy, and the leading-edge beam was stainless steel. The total exposed surface area was about 52 ft^2. As shown in the figure, the horizontal stabilizer was instrumented internally with 121 thermocouples, with an additional 11 thermocouples located on the outer surface of the torque box extending inboard from the main beam. All of this instrumentation was used for both flight and ground test measurements. A comprehensive report on the heating simulation on the stabilizer is available [1].

Infrared quartz lamps were used to provide heat flux for the aerodynamic flight heating simulation performed in the laboratory. As shown in Fig. 13, the lamps were mounted on polished stainless steel reflectors

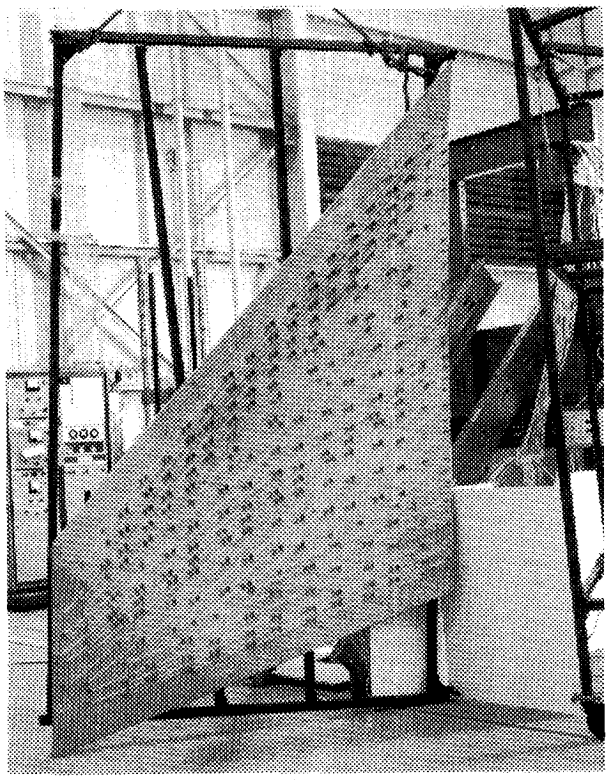

E-18908

Fig. 13 Quartz heater system for the X-15 horizontal stabilizer.

of the same shape and contour as the stabilizer; the reflectors were then positioned 5.5 $\pm$ 0.5 in. above and below the stabilizer to form the primary heater. The quartz heating lamps were distributed on the reflector with the highest densities over the main beam, leading-edge assembly, and trailing-edge beam. An analog closed-loop control system was used to regulate lamp power and produce a programmed temperature-time history on the stabilizer surface. Control feedback was provided by control thermocouples at particular locations on the test article.

The distribution of lamps into zones (areas to be controlled by one thermocouple) is shown in Fig. 14. All of the quartz lamps in any one zone were wired together in parallel. The distribution of lamps within

each zone helped provide the proper distribution of heat flux over the stabilizer surface. Figure 14(a) shows the initial configuration, which consisted of 222 12-in. 1000-W lamps for each reflector. The size of the 22

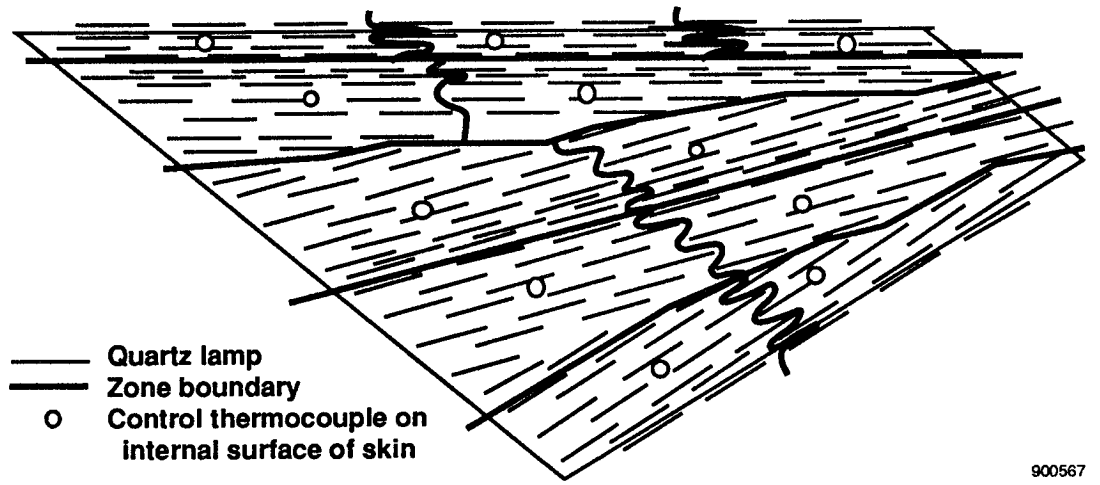

(a) Initial.

Fig. 14 Lamp zoning for the X-15 horizontal stabilizer heating system.

control zones ranged from approximately 1.0 ft^2 to 3.9 ft^2, and the number of lamps in each zone ranged from 11 to 26.

Preliminary heating-test results indicated that it would be necessary to increase the number of control zones over the stabilizer surface to better simulate the flight-measured temperature distribution. Additional lamps were also required at the leading edge and root rib. The final lamp zoning configuration, shown in Fig. 14(b), consisted of 496 quartz lamps divided into 36 control zones for both the upper and lower surfaces.

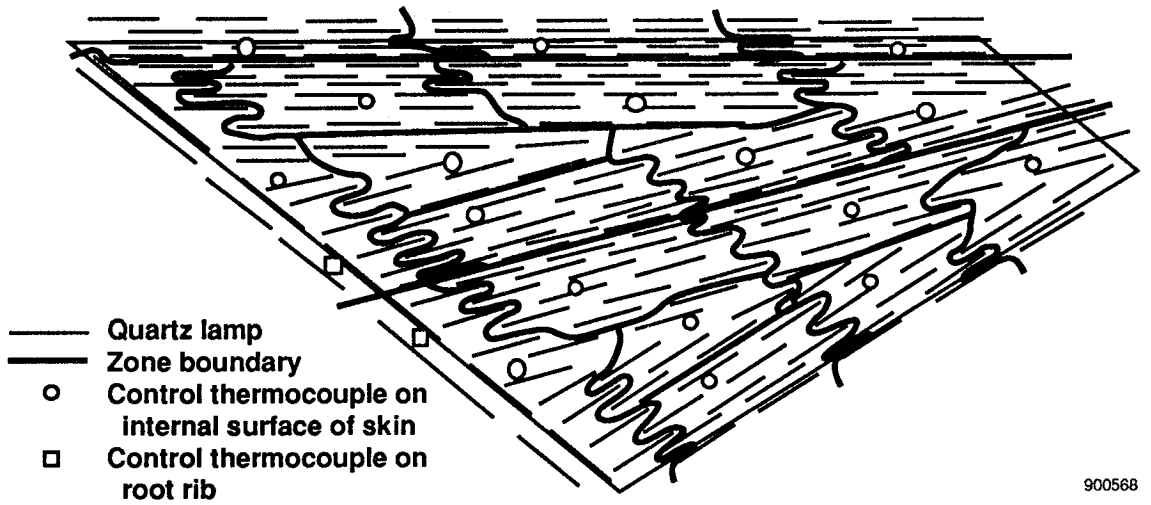

(b) Final.

Fig. 14 Concluded.

Figure 15 shows an edge view of the horizontal stabilizer with the quartz heater system in place around it. Toward the left of the figure, the additional quartz lamps required to heat the leading edge can be seen. Because of the steep temperature gradient going aft from the leading edge (left to right in the figure), dividers were placed between control zones to prevent cooler zones from being overheated by adjacent hotter zones.

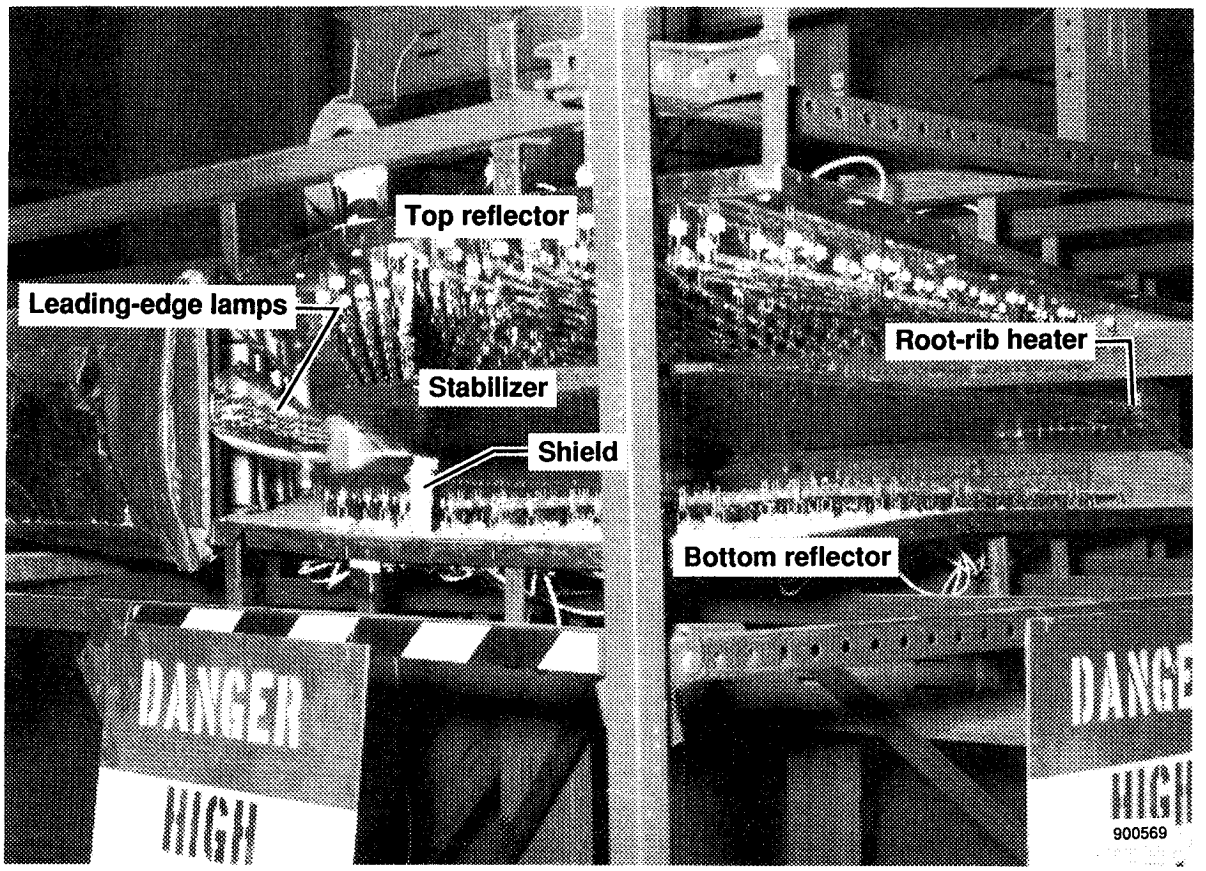

Fig. 15 Heater assembly for heating simulation on the X-15 horizontal stabilizer.

Even though zone sizes had been reduced, temperature differences within zones still existed, as shown in Fig. 16. Data are shown for two thermocouples (54 and 87). The thermocouples were installed to measure

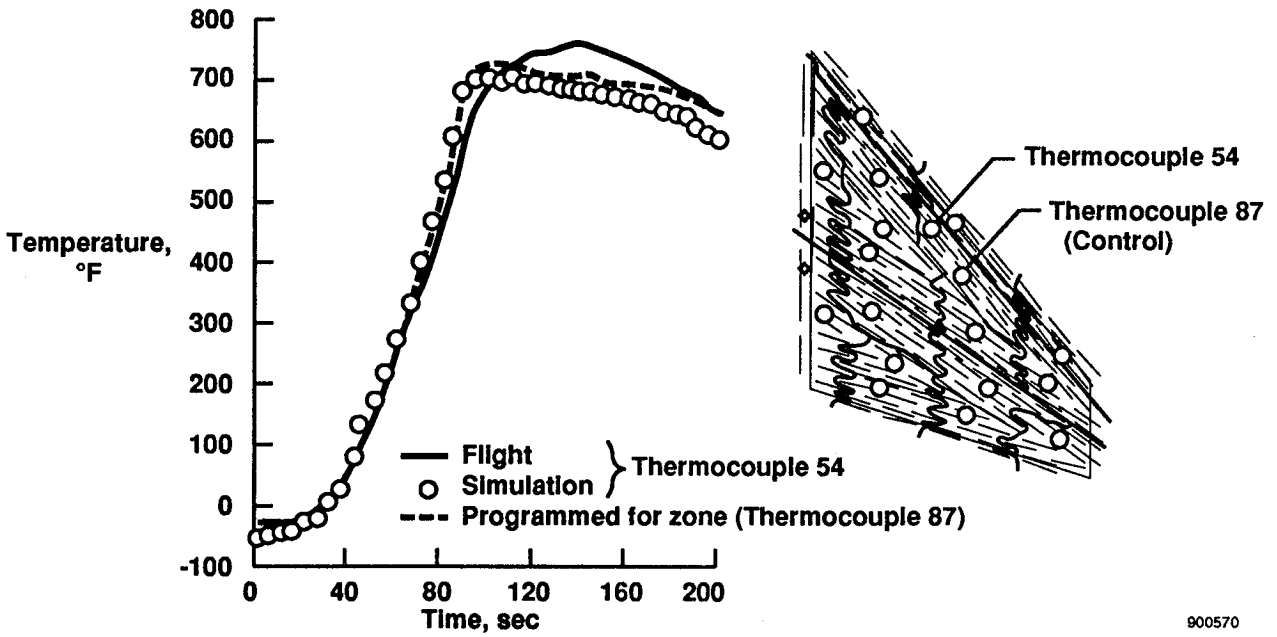

Fig. 16 Temperature variation within the heating zone that includes thermocouples 54 and 87.

both flight and ground test data. The flight profile of thermocouple 87 was programmed for heating the zone, hence, the flight data for this thermocouple are not shown. As shown in the figure, the simulation temperature profile for thermocouple 54 is slightly lower than the profile programmed (and flight measured) for control thermocouple 87. The flight-measured temperature profile for thermocouple 54 is considerably higher for a portion of the time history. This situation might have been improved by programming the average temperature or decreasing the zone size again.

The hypersonic wing test structure (HWTS) is a full-scale (85 ft^2 planform area) wing section designed for a Mach 8 research airplane concept. The structure was constructed with single-sheet, spanwise-stiffened beaded panels made of René 41 (Teledyne Allvac/Vasco Marketing, Monroe, NC) with heat shields on the external surfaces made of René 41 and TD NiCr. A detailed description of the structure is available [10]. Quartz lamp heaters were fabricated to heat the entire upper and lower surfaces to test this structure at the calculated Mach 8 temperatures (Fig. 17). The lower surface heater, as shown in Fig. 17(a), was divided into 47 thermal control zones in the final test configuration. The locations of the control thermocouples on the heat shield surface are shown. Gaps were provided in the heater to accommodate mechanical load attachments to the wing structure for combined heating and loading tests.

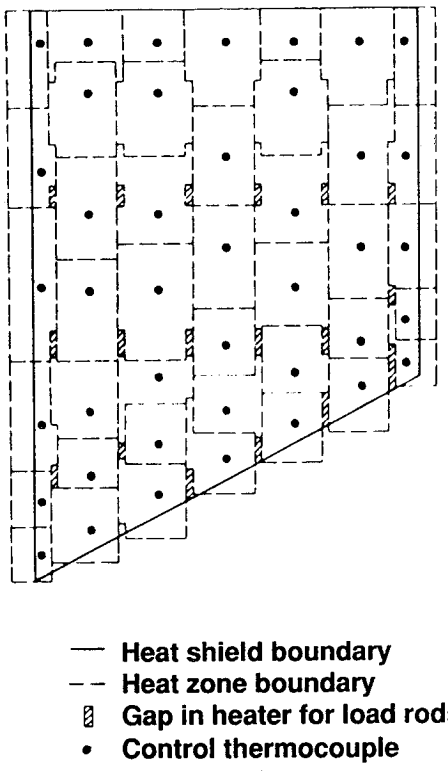

— Heat shield boundary
– – Heat zone boundary
▨ Gap in heater for load rods
• Control thermocouple

900571

(a) Final zones.

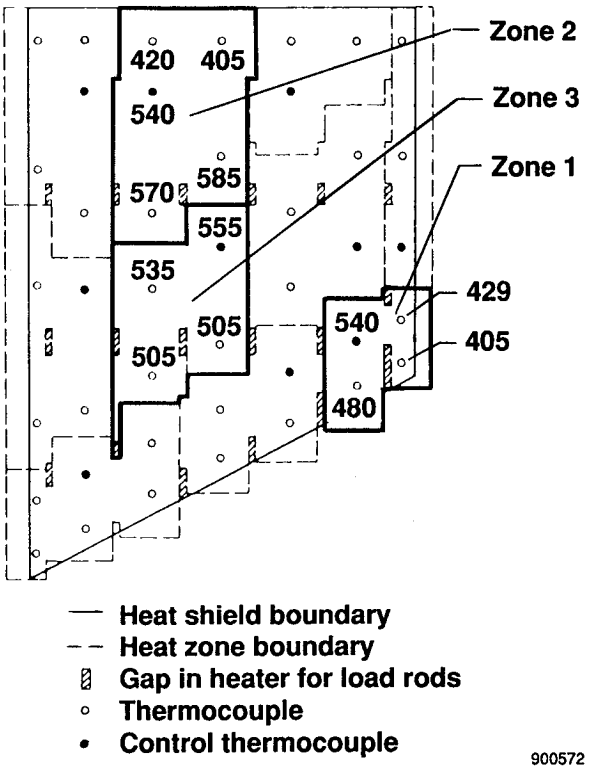

— Heat shield boundary
– – Heat zone boundary
▨ Gap in heater for load rods
○ Thermocouple
• Control thermocouple

900572

(b) Initial zones showing temperatures within the zones.

Fig. 17 Heating control zones for the hypersonic wing test structure, lower surface.

An initial heating test series was conducted on the HWTS using a limited number of analog thermal control channels. The control zone sizes and distribution on the lower surface are shown in Fig. 17(b). Note that the lamp distribution is uniform within each zone. All of the thermocouple instrumentation shown in Fig. 17(b) was utilized for temperature measurements, however, only those indicated by the solid symbols were needed for control purposes. The remainder of the thermocouple measurements provided data on temperature distributions within zones, which is also shown in the figure for three different control zones at steady-state conditions. Zones 1 and 2 show significant heat losses at the boundaries, most likely caused by convection and–or radiation losses. Zone 3 shows an internal control zone, that is, well away from boundary conditions. Although the temperature deviations of 50 °F within zone 3 are not as large as those in the first two zones, they are still large enough to cause anomalies between test and analysis.

In-flight aerodynamic heating is a function of the difference between the recovery temperature and the surface temperature. Laboratory radiant heating is a function of the fourth powers of the lamp temperature and the surface temperature. Because of this fundamental difference in heating, it is important that lamps be distributed to accommodate this variation within a control zone, particularly in locations where there is a significant heat sink. Consequently, a computer program [1] was written to calculate the surface flux distribution for a specified heater-lamp configuration. The program can address many variables as indicated in Fig. 18.

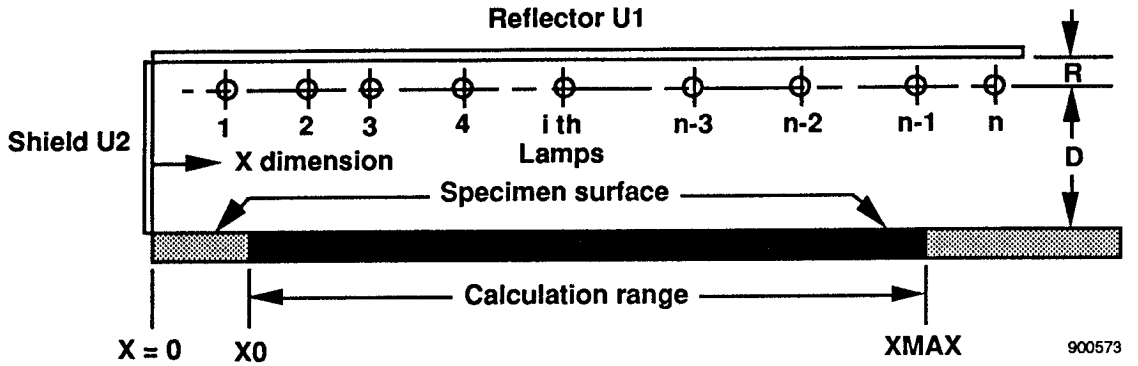

Fig. 18 Heater-specimen configuration for lamp flux computer program.

Lamp configuration data from the horizontal stabilizer test setup at a midspan station were entered into the lamp flux program for analysis. Figure 19 compares the net radiant flux required to maintain the flight-

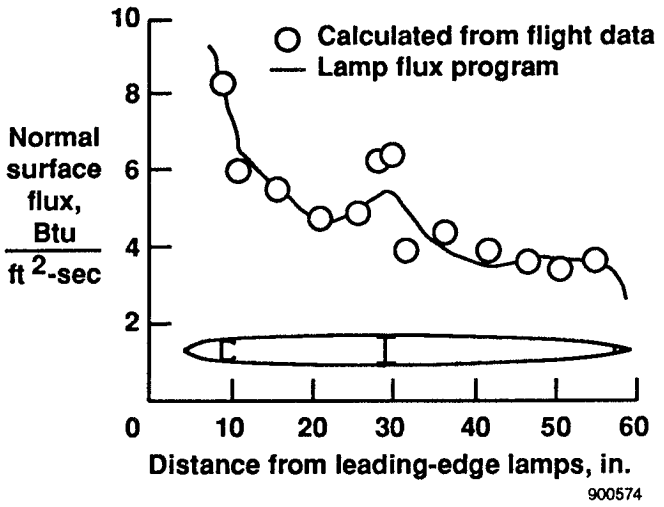

Fig. 19 Normal surface flux distribution on a cross section of the X-15 horizontal stabilizer 75 sec into the flight.

temperature time history with that provided by the lamps as computed by the program for a time 75 sec into the flight. A comparison of the calculated curve and the flight data indicates that the distribution is well-matched except at the main beam location. At that location, the structural discontinuity (that is, large heat sink) is not compensated for by a corresponding heat flux discontinuity. This heat flux discontinuity could be better simulated in the laboratory by adding separate control zones over the length of the spar and placing insulator shields between the lamp zones.

End effects on the boundaries of infrared heater systems can be a major source of temperature error. The problem and some potential solutions are shown in Fig. 20. The data for this figure were calculated using

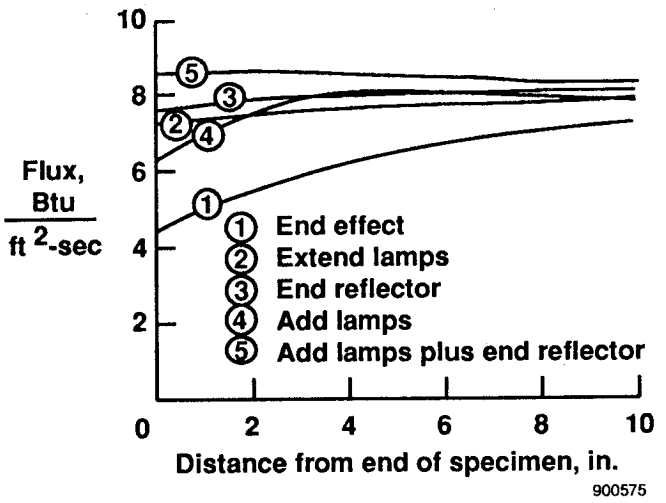

Fig. 20 Infrared heater end effects.

the lamp flux computer program discussed earlier (see Fig. 18). Figure 20 shows the calculated heat flux received by the first 10 in. of the test specimen for various reflector lamp arrangements. Curve 1 shows the heat flux when the reflector ends at $X = 0$, and there is no end reflector and no added lamps. Curve 4 is the same as curve 1 except lamps were added near $X = 0$. Curve 2 is the same as curve 1 except the reflector and lamps were extended 10 in. beyond the specimen surface. Curve 3 is the same as curve 1 except an end reflector was added and curve 5 is the same as curve 3 except that additional lamps were installed. This figure is not intended to present all the possible heater designs to eliminate or to minimize end effects. The results shown do illustrate that this is a very serious problem that must be considered when designing infrared radiation heaters. Based on the results shown in this figure, it can be concluded that as a minimum, the reflector must extend approximately 10 in. beyond the test specimen and that an end reflector is required if the heat loss resulting from end effects are to be kept to a reasonable amount.

Figure 21 demonstrates how the end-effect problem was solved for the root section of the X-15 horizontal stabilizer. This is a view looking forward at the trailing-edge beam and along the root rib of the stabilizer. End reflectors and additional lamps were added to the upper and lower heater systems, as shown in the figure. In addition, an independent heater was added to provide additional heat to the root rib.

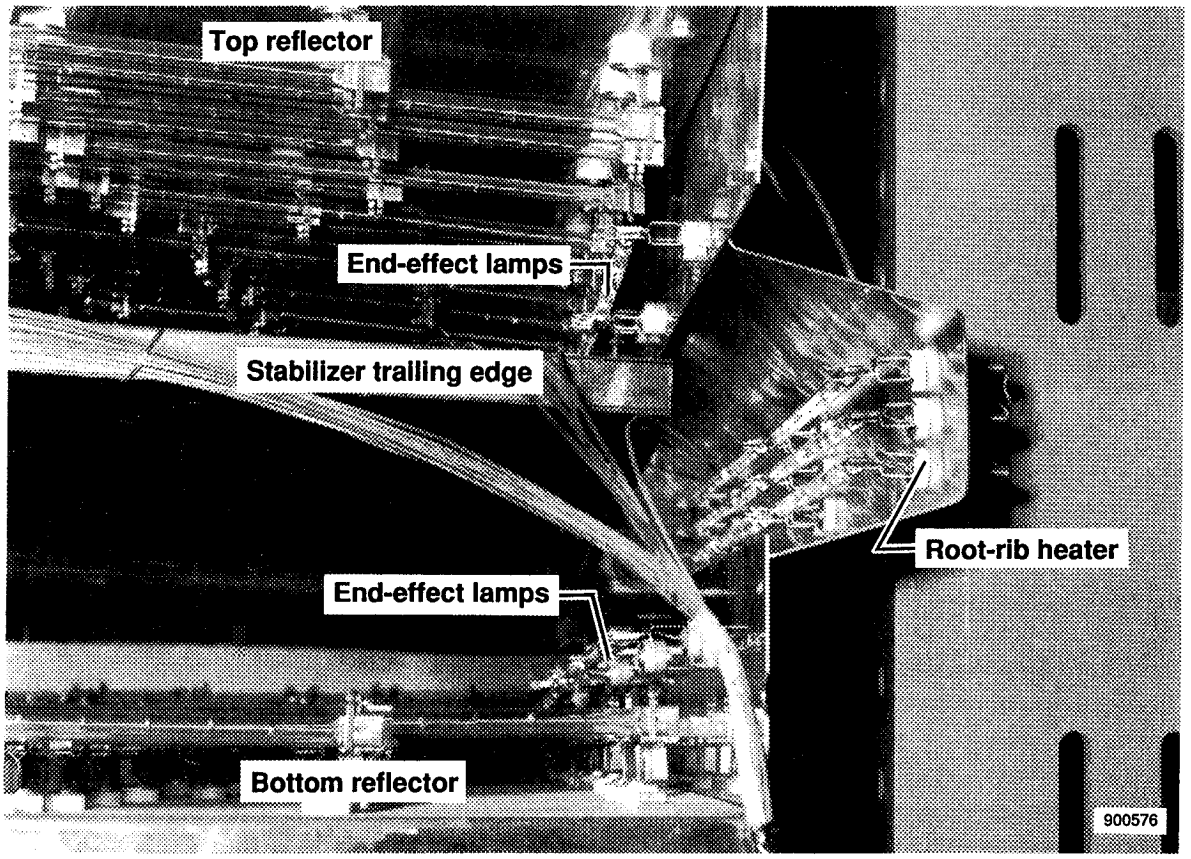

Fig. 21 X-15 horizontal stabilizer root-rib heater.

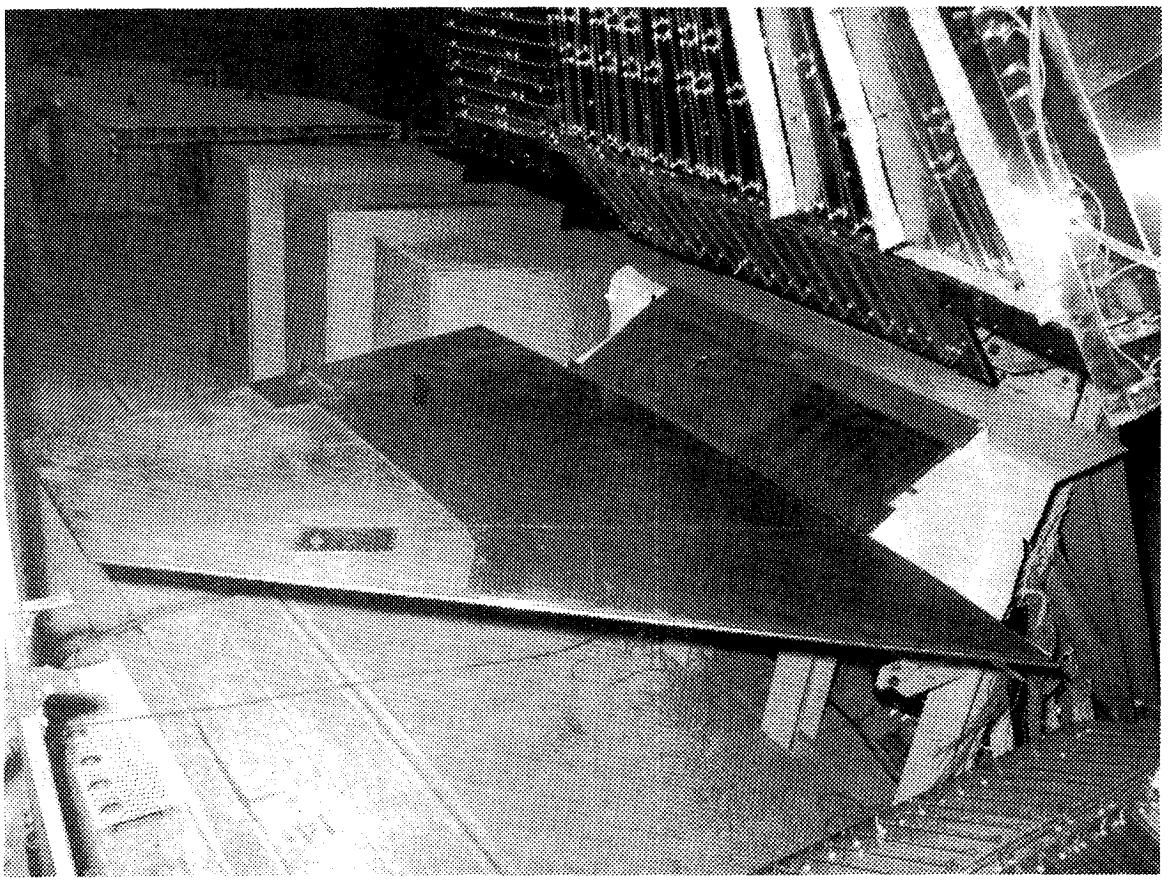

E-20336

Fig. 22 X-15 wing.

The X-15 wing, shown in Fig. 22, is a short-span, thin, low-aspect ratio, multispar structure. It has three main ribs: a root rib, a midspan rib and a tip rib. The leading edge is a segmented slug or heat sink having a constant radius. The wing-to-fuselage attachments consist of five A-frame assemblies which are an integral part of the wing. The wing skins, tip rib, front spar, and structure forward of the front spar are constructed of Inconel-X; the remainder of the wing structure is of titanium alloy. The wing is shown in the condition it was received in the laboratory, after removal from the aircraft. The nonuniformity of the wing-surface emissivity is obvious. A portion of the upper surface quartz heater system is shown in a raised or open position.

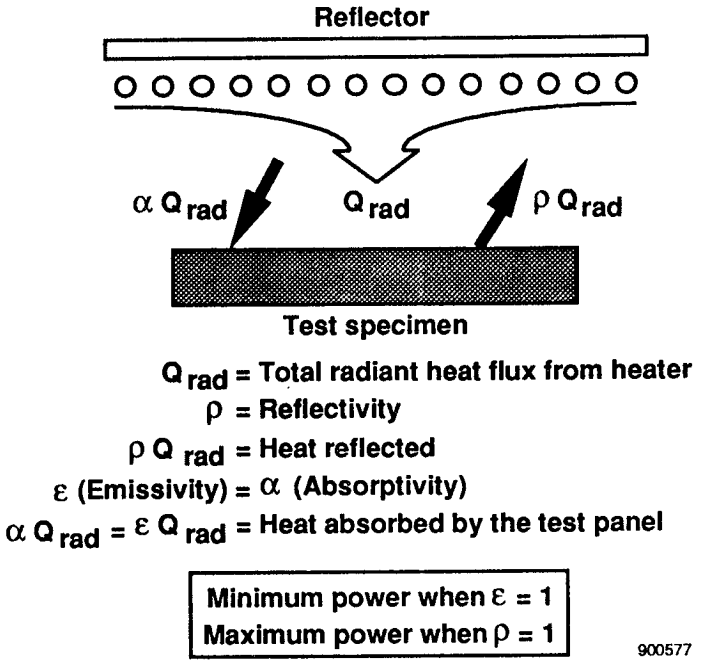

Fig. 23 Effect of surface emissivity on power.

The effects of surface emissivity on the power required for a radiation heating system is illustrated in Fig. 23. Part of the total radiant heat flux from the heater is absorbed by the test specimen and the remainder of the heat flux is reflected. The amount of the heat absorbed and reflected depends on the absorptivity and the reflectivity of the test specimen. Since absorptivity plus reflectivity equals 1.0, the amount of heat absorbed depends on the emissivity. Therefore, it is obvious that the minimum power required will occur when the emissivity of the test specimen is equal to 1.0. Likewise, the maximum power will be required when the reflectivity is 1.0. Consequently, the test specimen should have a uniform emissivity if consistent results are to be obtained from infrared heating tests.

Preliminary heating tests of the X-15 wing [2] showed discrepancies between the simulation temperatures measured within each zone and the calculated temperatures. It was decided that the lack of uniformity

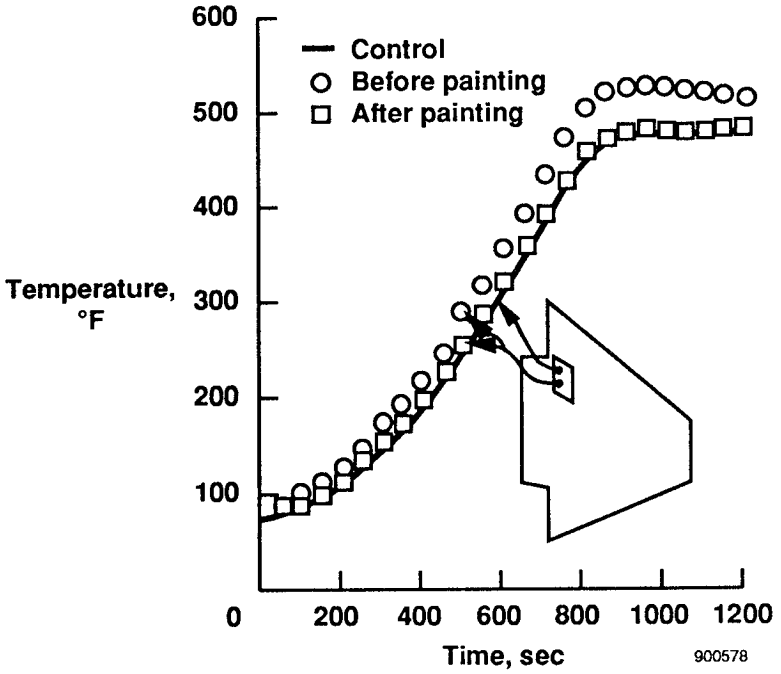

Fig. 24 X-15 wing test illustrating emissivity effects.

in the surface emissivity was the most likely problem, so the wing was painted with a fresh coat of high emissivity paint. Figure 24 shows the effect of the painted surface on measured temperatures. Before painting, the control thermocouple (solid line) was in an area of higher reflectivity than the area of the thermocouple shown with the circular symbols. This resulted in a large thermal gradient within the controlled zone. Gradients such as this produce unrealistic thermal stresses and corresponding test anomalies. After the wing was painted, the undesirable gradient was virtually eliminated.

Figure 25 demonstrates how high emissivity paint can be useful for reducing heater system end effects. A quartz heater system with a ceramic reflector was used in an attempt to heat the upper surface of a honeycomb

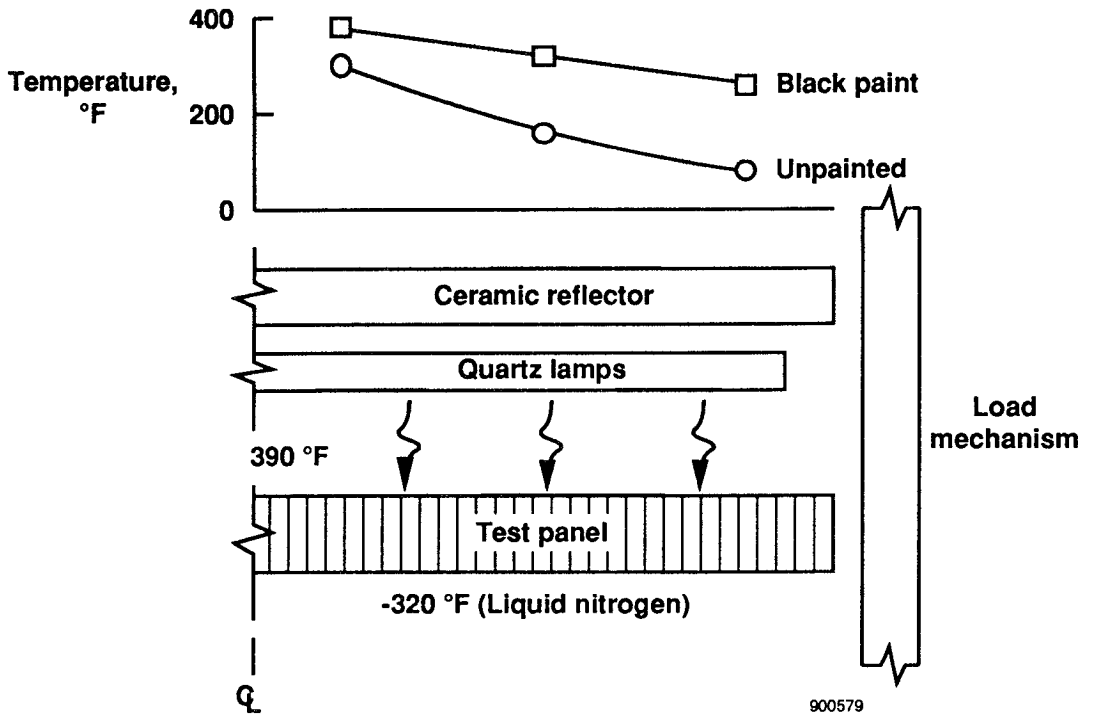

Fig. 25 Emissivity effect on a honeycomb panel.

panel [11] to a constant 390 °F. The lower panel surface was held at −320 °F with liquid nitrogen. As can be seen, the heater system could not be extended past the edge of the panel because of the presence of a loading mechanism. Controlling the panel centerline to 390 °F, with the panel unpainted, produced a severe temperature gradient across the panel. The outer one-quarter of the panel upper surface was painted with black paint, and the subsequent repeat test still showed a temperature gradient, but one which was much less severe. Thus, this single change produced a more uniform upper surface temperature distribution.

SUMMARY

Thermal structural testing is a complex, time-consuming, and costly process, especially when attempting to provide high-quality experimental data. Several key elements of hot structures testing were addressed including data acquisition and control, temperature and strain measurement, and quartz lamp heater systems. The following summarizes the major points of this paper.

Extensive temperature measurement is the key to understanding and evaluating hot structures test results. Thermal control zones must be kept to a minimum size to achieve good-quality temperature distributions over the entire test article. The infrared heater system may have to be tailored to provide the required heat flux distribution within a control zone. Proper test article surface emissivity is critical to thermal simulation with infrared heating systems. Special attention must be given to the treatment of boundary conditions to avoid troublesome temperature distributions.

Temperatures were measured from −320 °F to 2600 °F using thermocouples. Strains have been measured from −320 °F to 1500 °F using a combination of foil, weldable, and capacitive strain gages. Accurate apparent strain data are essential to insure correct strain measurements at temperatures other than room temperature. The iron-chromium-aluminum (Fe-Cr-Al) gages appear to offer strain measurement at temperatures up to 1900 °F in limited applications.

The data acquisition and control system (DACS) can be considered the "heart" of hot structural testing, because accurate thermal control and clean data recording are critical elements to effective elevated-temperature testing. The DACS has provided the custom environment needed to conduct tests without data contamination to mislead the test data analyst.

With the renewed interest in hypersonic flight, unique test articles necessary to mature hot structures technology will demand the development of newer and broader test techniques. Of special note will be an ever greater need to perform combined thermal–mechanical tests on structures containing hydrogen.

REFERENCES

[1] Fields, Roger A., and Vano, Andrew, *Evaluation of an Infrared Heating Simulation of a Mach 4.63 Flight on an X-15 Horizontal Stabilizer*, NASA TN D-5403, 1969.

[2] Fields, Roger A., Olinger, Frank V., and Monaghan, Richard C., *Experimental Investigation of Mach 3 Cruise Heating Simulations on a Representative Wing Structure for Flight-Loads Measurements*, NASA TN D-6749, 1972.

[3] Fields, Roger A., *A Study of the Accuracy of a Flight-Heating Simulation and Its Effect on Load Measurement*, NASA TN D-5741, 1970.

[4] Monaghan, Richard C., and Fields, Roger A., *Experiments to Study Strain-Gage Load Calibrations on a Wing Structure at Elevated Temperatures*, NASA TN D-7390, 1973.

[5] Reardon, Lawrence F., *Evaluation of a Strain-Gage Load Calibration on a Low-Aspect-Ratio Wing Structure at Elevated Temperature*, NASA TP-2921, 1989.

[6] *NASA YF-12 Flight Loads Program*, NASA TM X-3061, 1974.

[7] *Workshop on Correlation of Hot Structures Test Data with Analysis*, NASA CP-3065, 1990.

[8] Zamanzadeh, Behzad, Trover, William F., and Anderson, Karl F., "DACS II - A Distributed Thermal/Mechanical Loads Data Acquisition and Control System," International Telemetering Conference/'87, Instrument Society of America, San Diego, CA, July 15, 1987.

[9] Lemcoe, M.M., "Characterization of BCL, Chinese, and Dentronics High Temperature Strain Gages," Eighth National Aero-Space Plane Technology Symposium," *vol. VI-Structures*, NASP CP-8051, 1990, paper no. 42, pp. 123–147.

[10] Fields, Roger A., Reardon, Lawrence F., and Siegel, William H., *Loading Tests of a Wing Structure for a Hypersonic Aircraft*, NASA TP-1596, 1980.

[11] Shideler, J.L., Swegle, A.R., and Fields, R.A., "Honeycomb Sandwich Structure for Future Space Transportation Systems with Integral Cryogenic Tankage," *J. of Spacecraft and Rockets*, vol. 21, no. 3, May–June 1984, pp. 246.

NASA
National Aeronautics and Space Administration

Report Documentation Page

1. Report No.	2. Government Accession No.	3. Recipient's Catalog No.
NASA TM-101727		

4. Title and Subtitle	5. Report Date
Techniques for Hot Structures Testing	November 1990
	6. Performing Organization Code

7. Author(s)	8. Performing Organization Report No.
V. Michael DeAngelis and Roger A. Fields	H-1664
	10. Work Unit No.
	RTOP 505-63-31

9. Performing Organization Name and Address	11. Contract or Grant No.
NASA Ames Research Center Dryden Flight Research Facility P.O. Box 273, Edwards, CA 93523-0273	
	13. Type of Report and Period Covered
12. Sponsoring Agency Name and Address	Technical Memorandum
National Aeronautics and Space Administration Washington, DC 20546-0001	14. Sponsoring Agency Code

15. Supplementary Notes

Prepared for presentation at the First Thermal Structures Conference, University of Virginia, Charlottesville, Virginia, November 13–15, 1990.

16. Abstract

The Aerostructures Branch personnel at NASA Ames Research Center, Dryden Flight Research Facility have been involved with hot structures testing since the early 1960's beginning with the Mach 6, X-15 airplane. Early hot structures test programs at NASA Ames-Dryden focused on operational testing required to support the X-15 flight test program, and early hot structures research projects focused on developing laboratory test techniques to simulate flight thermal profiles. More recent efforts involved numerous large and small hot structures test programs that served to develop test methods and measurement techniques to provide data that promoted the correlation of test data with results from analytical codes. In November 1988, the Aerostructures Branch at NASA Ames-Dryden, with participation from Langley Research Center, sponsored a workshop that focused on the correlation of hot structures test data with analysis. This paper draws limited material from the workshop and provides a more formal documentation of topics that focus on hot structures test techniques employed at the NASA Ames-Dryden Aerostructures Branch. Topics covered include the data acquisition and control of testing, the quartz lamp heater systems, current strain and temperature sensors, and hot structures test techniques used to simulate the flight thermal environment in the laboratory.

17. Key Words (Suggested by Author(s))	18. Distribution Statement
Flight heating simulation Flight loads Hot structures Radiant heating	Unclassified-Unlimited Subject category - 05

19. Security Classif. (of this report)	20. Security Classif. (of this page)	21. No. of Pages	22. Price
Unclassified	Unclassified	28	A03

NASA FORM 1626 OCT 86

For sale by the National Technical Information Service, Springfield, Virginia 22161